Simultaneous magnetic resonance imaging of ventilation distribution and gas uptake in the human lung using hyperpolarized xenon-129

John P. Mugler III[a,1], Talissa A. Altes[a], Iulian C. Ruset[b,c], Isabel M. Dregely[c], Jaime F. Mata[a], G. Wilson Miller[a], Stephen Ketel[b], Jeffrey Ketel[b], F. William Hersman[b,c], and Kai Ruppert[a]

[a]Center for In Vivo Hyperpolarized Gas MR Imaging, Department of Radiology, University of Virginia, Charlottesville, VA 22908; [b]Xemed LLC, Durham, NH 03824; and [c]Department of Physics, University of New Hampshire, Durham, NH 03824

Edited* by William Happer, Princeton University, Princeton, NJ, and approved November 1, 2010 (received for review August 23, 2010)

Despite a myriad of technical advances in medical imaging, as well as the growing need to address the global impact of pulmonary diseases, such as asthma and chronic obstructive pulmonary disease, on health and quality of life, it remains challenging to obtain in vivo regional depiction and quantification of the most basic physiological functions of the lung—gas delivery to the airspaces and gas uptake by the lung parenchyma and blood—in a manner suitable for routine application in humans. We report a method based on MRI of hyperpolarized xenon-129 that permits simultaneous observation of the 3D distributions of ventilation (gas delivery) and gas uptake, as well as quantification of regional gas uptake based on the associated ventilation. Subjects with lung disease showed variations in gas uptake that differed from those in ventilation in many regions, suggesting that gas uptake as measured by this technique reflects such features as underlying pathological alterations of lung tissue or of local blood flow. Furthermore, the ratio of the signal associated with gas uptake to that associated with ventilation was substantially altered in subjects with lung disease compared with healthy subjects. This MRI-based method provides a way to quantify relationships among gas delivery, exchange, and transport, and appears to have significant potential to provide more insight into lung disease.

gas exchange | pulmonary function | pulmonary ventilation

Lung diseases, such as asthma and chronic obstructive pulmonary disease (COPD), have a tremendous impact on health and quality of life both in the United States and worldwide. For example, COPD, the fourth-leading cause of death in the United States, is the only major cause of death for which the age-adjusted death rate has increased in recent years. Progress in understanding the genetic and molecular pathways involved in such diseases brings a growing need for improved tools to characterize lung function for such applications as coupling genetic subtypes to phenotype expression, monitoring functional response to new treatments, and aiding in the rapid development of new respiratory drugs. But despite the many recent advances in medical-imaging technology, there remains no imaging approach suitable for routine application in humans that provides regional depiction and quantification of the most basic physiological functions of the lung: gas delivery to the alveolar airspaces and gas uptake by the lung parenchyma and blood.

The use of MRI with the hyperpolarized noble gases helium-3 (He3) and xenon-129 (Xe129) has led to the development of unique strategies for evaluating lung structure and function (1). In particular, xenon's relatively high solubility in biological tissues (2), along with its exquisite sensitivity to its environment that results in an enormous range of chemical shifts upon solution (3), make hyperpolarized Xe129 particularly attractive for exploring certain characteristics of lung function, such as gas exchange and uptake (4, 5), not accessible with the use of hyperpolarized He3. Upon inhalation, Xe129 gives rise to multiple MRI spectral peaks in the lung (6–9), each associated with a physically different compartment. Most Xe129 resides in the lung airspaces ("gas-phase" xenon), and is associated with a single large peak, whereas ~1–2% is dissolved in the lung parenchyma and blood ("dissolved-phase" xenon) and gives rise to two or more smaller peaks at chemical shifts of about 200 ppm from the gas peak (6–9). The small pool of dissolved-phase xenon exists in dynamic equilibrium with xenon in the airspaces; driven by diffusion, atoms in the gas and dissolved compartments continually exchange. The quantitative characteristics of the process of gas exchange and uptake are determined by parameters of physiological relevance, such as the thickness of the blood–gas barrier (5); thus, measurements that quantify this process potentially offer a wealth of information on the functional status of the healthy and diseased lung.

Images that directly depict the dissolved-phase compartments are required to take full advantage of the information offered by dissolved-phase Xe129 MRI. Although detection of the dissolved-phase signal in the human lung was demonstrated in early studies, the associated signal-to-noise ratios were insufficient to permit acquisition of dissolved-phase images (8). Such images were subsequently acquired in animals using repeated inhalations of hyperpolarized Xe129 (5, 10, 11), but with current technology, a multiple-inhalation approach is not feasible in humans. However, with improvements in gas-polarization hardware (12), liter quantities of hyperpolarized Xe129 can be obtained with sufficient polarization to make direct dissolved-phase imaging in humans feasible during a single breath-hold period. Recently, Cleveland et al. (13) produced breath-hold images of the dissolved phase in humans following inhalation of 1 L of Xe129. Nonetheless, because the absolute dissolved-phase signal intensity has no physical meaning, measurement of the dissolved-phase signal alone cannot make the critical distinction between pathological alterations in ventilation (gas delivery to the airspaces) versus those in tissue microstructure or blood flow. Thus, there is a need for an imaging approach suitable for application in humans that permits quantification of the dissolved-phase signal and, ideally, also permits regional assessment of both ventilation and gas uptake from a single, short acquisition that can be easily tolerated by subjects with compromised respiratory function due to disease.

The large difference in chemical shift, and hence resonant frequency, between gas-phase and dissolved-phase Xe129 provides an opportunity to capture both components in the same image, thus potentially yielding from a single breath-hold ac-

Author contributions: J.P.M., T.A.A., I.M.D., J.F.M., G.W.M., F.W.H., and K.R. designed research; J.P.M., T.A.A., I.C.R., I.M.D., J.F.M., S.K., J.K., and K.R. performed research; I.C.R., G.W.M., and F.W.H. contributed new reagents/analytic tools; J.P.M., T.A.A., F.W.H., and K.R. analyzed data; and J.P.M., T.A.A., F.W.H., and K.R. wrote the paper.

Conflict of interest statement: I.C.R., S.K., and J.K. are employees of Xemed LLC, manufacturer of the prototype xenon-129 gas polarization system used for the imaging studies. F.W.H. is founder and CEO of Xemed LLC.

*This Direct Submission article had a prearranged editor.

Freely available online through the PNAS open access option.

[1]To whom correspondence should be addressed. E-mail: John.Mugler@virginia.edu.

This article contains supporting information online at www.pnas.org/lookup/suppl/doi:10.1073/pnas.1011912107/-/DCSupplemental.

quisition simultaneous depiction of the 3D distributions of the gas after inhalation and of the fraction of gas exchanging into the lung parenchyma and blood. Simultaneous acquisition of a ventilation image with matched spatial resolution provides the ideal basis for normalizing the dissolved-phase signals, allowing regional quantification of gas uptake by calculating the ratio of the dissolved-phase and gas-phase signals. This ratio parameter, which is likely to be sensitive to pathological changes in lung function, may offer insight into the physiological effects of such diseases as asthma and COPD. Here we demonstrate the feasibility of such a method for simultaneous MRI of ventilation distribution and gas uptake, and present preliminary results from healthy and diseased human lung.

Results

Simultaneous MRI of Ventilation Distribution and Gas Uptake. We developed an MRI acquisition method (pulse sequence) to generate MRI images that show, side-by-side, Xe129 in the lung airspaces and Xe129 dissolved in the lung parenchyma and blood (Fig. 1). The method was based on an established approach (radiofrequency-spoiled gradient-echo imaging) for rapid MRI, allowing completion of a 2D acquisition of the lung in a few seconds and a 3D acquisition in less than 20 s. Because the amount of Xe129 in the dissolved-phase compartments is much less than that in the airspaces, and because Xe129 in the airspaces acts as a reservoir for the dissolved-phase compartments, we designed an excitation radiofrequency pulse for the pulse sequence that resulted in a relatively high degree of excitation (i.e., a high "flip angle") for Xe129 in the dissolved-phase compartments, but a relatively low degree of excitation for Xe129 in the airspaces (Fig. 1*B*). We chose sampling characteristics for the pulse sequence (*Materials and Methods*) that provided complete separation of the gas and dissolved components along one of the axes (specifically, the "frequency-encoding direction") of the image (Fig. 1*C*).

Subject Characteristics and Tolerance of Imaging Procedures. We enrolled 11 human subjects for simultaneous MRI of ventilation distribution and gas uptake, including 6 healthy subjects, 3 subjects with clinically diagnosed asthma, and 2 subjects with clinically diagnosed smoking-related COPD (Table 1). Immediately before MRI, we measured standard lung functional indices based on spirometry, including forced vital capacity (FVC) and absolute and percent-predicted forced expiratory volume in 1 s (FEV_1). Spirometric indices were in the normal range ($FEV_1 \geq 80\%$ predicted and $FEV_1/FVC \geq 70\%$) for the healthy subjects, but below the normal range for the subjects with lung disease (Table 1).

All subjects were able to inhale the hyperpolarized Xe129 gas and hold their breath for the required time, which ranged between 2 s and 18 s. We performed a total of 20 simultaneous gas-phase, dissolved-phase Xe129 acquisitions in the 11 subjects; we imaged one of the healthy subjects in two separate sessions (Table S1). For each subject, we acquired 2D projection images (i.e., spatially resolved in two directions and integrated over the thickness of the lung in the remaining direction), 3D images (i.e., spatially resolved in all three directions), or both (Table 1). The xenon inhalations were well tolerated by all subjects, although 6 of the 11 subjects experienced mild transient central nervous system side effects, such as slight tingling or lightheadedness, with one or more of the xenon inhalations.

Ventilation Distribution and Gas Uptake in Healthy Subjects. As expected, the 2D projection acquisitions demonstrated a spatially uniform distribution of gas-phase Xe129 signal, indicating uniform ventilation of the airspaces, as well as a spatially uniform distribution of dissolved-phase Xe129 signal, indicating uniform uptake of hyperpolarized xenon by the lung tissue and blood (Fig. 1*D*, subject 1). The 3D acquisitions in healthy subjects also demonstrated generally uniform distributions of gas-phase and dissolved-phase signal intensities throughout the lung volume (Fig. 2, top panel of

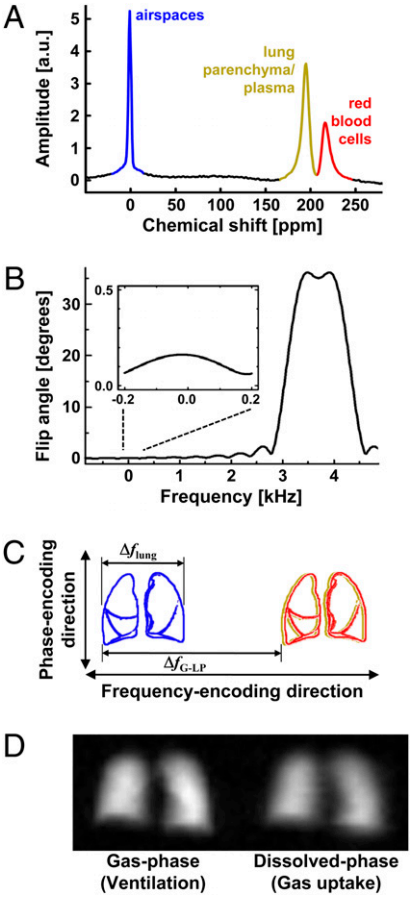

Fig. 1. Relationships between the spectral peaks of Xe129 and the excitation and frequency-encoding characteristics of an appropriately designed MRI pulse sequence illustrate how to take advantage of the large chemical shift difference between gas-phase and dissolved-phase Xe129 to simultaneously acquire images of ventilation distribution (gas phase) and gas uptake (dissolved phase). (*A*) Representative spectrum of Xe129 in a healthy human lung showing peaks at 0, 198, and 218 ppm, corresponding to Xe129 in the lung airspaces, dissolved in lung parenchyma and blood plasma, and bound to hemoglobin in red blood cells, respectively. (*B*) For simultaneous imaging of the gas and dissolved components of Xe129, the center frequency of the radio-frequency pulse is chosen so that the main lobe of the frequency response covers the two dissolved peaks, and the pulse duration is chosen so that the central region of a side lobe corresponds to the gas-phase peak (*Inset*). (*C*) Dissolved-phase and gas-phase components are separated along the frequency-encoding direction of the image for appropriately selected pulse-sequence parameter values. (*D*) A representative coronal 2D projection image of the healthy lung (subject 1) demonstrates simultaneous depiction of uniform distributions of ventilation following inhalation and gas uptake.

the central six images from a coronal 3D acquisition in subject 8; Fig. S1, central eight images from an axial 3D acquisition in subject 9). Nonetheless, in healthy subjects, the dissolved-phase signal intensity was noticeably higher in the posterior portion of the lung than in the anterior portion (Fig. 2, *Top*).

We made an incidental finding of a 1-cm pulmonary nodule in the upper left lung of one of the healthy subjects (subject 3). Multiplanar image reconstructions (Fig. 3, *A*–*C*) from a 3D acquisition in this subject illustrated the correspondence between a ventilation defect (i.e., a region of absent signal) in the gas-phase Xe129 component and a focal region of elevated dissolved-phase signal intensity. A coronal proton MRI image (Fig. 3*D*) at the location of the focal high signal intensity in the dissolved-phase component revealed a well-circumscribed nodule in

Table 1. Demographic information, spirometry, and types of MRI acquisition for each subject

			Subject data				
Experiment no.	Subject no.	Age, y	Sex	FEV_1, % predicted	FEV_1/FVC, %	Health status	MRI acquisition type
1	1	21	F	90	80	Healthy	2D projection
2	2	67	M	36	49	Asthma	2D projection
3	3	21	F	104	80	Healthy	3D
4	3	21	F	108	82	Healthy	2D projection, 3D
5	4	63	F	80	66	COPD	2D projection
6	5	25	F	84	88	Healthy	2D projection
7	6	19	F	56	67	Asthma	2D projection
8	7	48	F	68	60	Asthma	2D projection, 3D
9	8	19	F	112	84	Healthy	3D
10	9	20	F	96	81	Healthy	3D
11	10	54	F	81	66	COPD	3D
12	11	19	F	104	84	Healthy	3D

the lung. This subject had participated in several previous research MRI studies. A retrospective examination of these studies revealed that the nodule had been absent in October 2008 but present in January 2009. During the intervening period, the subject had traveled to Central America as part of a medical mission. Although a number of colleagues on this trip developed symptomatic respiratory infections, our subject reported no respiratory symptoms; however, the rapid development of this nodule suggests an inflammatory/infectious etiology, possibly an incidental subclinical pulmonary infection acquired during the trip. A subsequent tuberculin skin test was negative. We hypothesize that inflammation associated with the nodule was responsible for focal accumulation of dissolved-phase Xe129 and hence the region of high signal intensity in the dissolved-phase component. Of note, this subject had otherwise homogeneous gas-phase and dissolved-phase images, similar to those for the other healthy subjects.

Ventilation Distribution and Gas Uptake in Subjects with Lung Disease. In the five subjects with lung disease, both the gas-phase and dissolved-phase components demonstrated nonuniform signal distributions. Although the gas distribution modulates the amount of Xe129 available for exchange, the signal intensity variations in the dissolved-phase components of the images were similar to but, importantly, not identical to those in the corresponding gas-phase components [Fig. 2, *Top* (subject 8, healthy) versus *Middle* (subject 7, asthma) and *Bottom* (subject 10, mild COPD), with identical acquisition parameters used for the three subjects].

We found numerous ventilation defects in the gas-phase Xe129 component of the images for the subjects with lung disease, for example, a ventilation defect in the gas-phase component for subject 7 (asthma) that had an associated defect in the dissolved-phase component (Fig. 2, *Middle*, arrowheads). The bright band of signal seen just below this defect in the dissolved-phase component was not present in the gas-phase component, however.

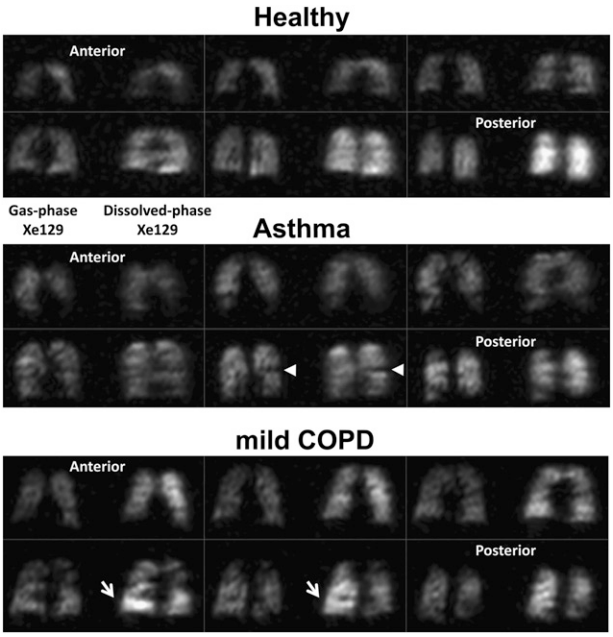

Fig. 2. 3D coronal acquisitions of the whole lung in subject 8 (healthy), subject 7 (asthma), and subject 10 (mild COPD) show marked spatial variations in ventilation and gas uptake in the subjects with asthma or COPD compared with generally uniform distributions in the healthy subject. Each panel shows the central six 20-mm-thick Xe129 images from the respective acquisition. For the subject with asthma, arrowheads indicate signal dropout at the location of a ventilation defect; a band of elevated signal is seen just below this defect in the dissolved-phase component. For the subject with mild COPD, arrows indicate regions of elevated signal intensity in the dissolved-phase component. MRI pulse-sequence parameters for all acquisitions include repetition time (TR), 50 ms; echo time (TE), 2.8 ms; flip angle at dissolved phase, 20°; bandwidth, 110 Hz/pixel (6.2 ppm/pixel); and spatial resolution, 12 × 12 × 20 mm.

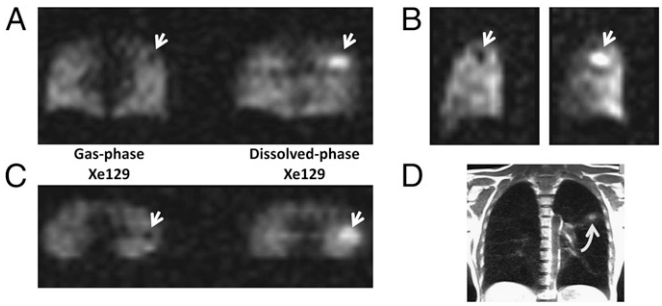

Fig. 3. Dissolved-phase Xe129 accumulated in the pulmonary nodule that was incidentally found in subject 3 (healthy). (*A–C*) Coronal (*A*), sagittal (*B*), and axial (*C*) reconstructions from a 3D acquisition highlighting the correspondence between the focal region of elevated dissolved-phase signal intensity in the upper left lung and a ventilation defect (arrows). (*D*) Coronal proton MRI image showing a 1-cm pulmonary nodule (curved arrow) at the same location. MRI pulse-sequence parameters for the 3D acquisition included TR, 35 ms; TE, 2.8 ms; flip angle at dissolved phase, 16°; bandwidth, 110 Hz/pixel (6.2 ppm/pixel); and spatial resolution, 12 × 12 × 12 mm.

In subject 10 (mild COPD), the signal intensity of the dissolved-phase component in the anterior portion of the lung (Fig. 2, *Bottom*, first two images) was clearly higher than that for the corresponding gas-phase component, whereas the signal intensities for the gas-phase and dissolved-phase components were similar in the anterior portion of the lung in the healthy subjects (e.g., Fig. 2, *Top*, first two images). Further, the dissolved-phase component in subject 10 showed pronounced variations in signal intensity that were not matched by variations of the same magnitude in the gas-phase component (Fig. 2, *Bottom*, arrows).

Ratio of Dissolved-Phase to Gas-Phase Xe129. We calculated the ratio of the signal intensities for dissolved-phase Xe129 to the signal intensities for gas-phase Xe129 in the four subjects in whom 3D acquisitions were performed using identical acquisition parameters. From these results, we calculated the mean values for the ratio on a slice-by-slice basis (Fig. 4). These data correspond to the images for subjects 7, 8, and 10 (Fig. 2), as well as those for subject 11 (healthy); the volume of gas inhaled was 0.74 L for subjects 7, 8, and 10 and 1.47 L for subject 11. In the two healthy subjects, the ratio increased monotonically from the anterior portion to the posterior portion of the lung (Fig. 4). Healthy subject 11 had markedly higher ratios in the most posterior slices compared with healthy subject 8 despite having inhaled a larger volume of gas (*Discussion*); this might be attributable to the two subjects' differing total lung volumes or differing relative degrees of lung inflation at the start of inhalation. The anterior-posterior variation in the ratio is consistent with the analogous change noted above in the dissolved-phase signal intensity along the anterior-posterior direction in healthy subjects. For subject 7 (asthma), the ratio in the anterior portion of the lung was similar to that in the healthy subjects, but the increase in the ratio from anterior to posterior was much smaller than that in the healthy subjects. In contrast, in subject 10 (mild COPD), the ratio in the anterior portion of the lung was markedly elevated compared with that in the healthy subjects and subject 7 and tended to slightly decrease, rather than increase, along the anterior-posterior direction.

Discussion

We have demonstrated the feasibility of using MRI of hyperpolarized Xe129 to acquire images in a single short breath-hold period lasting less than 20 s that simultaneously depict ventilation distribution and gas uptake in the human lung with matched spatial resolution. The distributions of both ventilation and gas uptake were overall spatially uniform in healthy subjects, as expected. Nonetheless, 3D acquisitions revealed a gradient in dissolved-phase signal intensity along the anterior-posterior direction, consistent with the observation of Cleveland et al. (13) and likely due to the well-described gravity-dependent gradient in lung tissue density from anterior to posterior in the supine position. Subjects with lung disease showed spatial variations in ventilation, as expected based on published studies using hyperpolarized He3 MRI (14–17), as well as in gas uptake, although the variations in gas uptake differed from the variations in ventilation in many regions of the lung. This suggests that the gas uptake component as measured by this technique is not simply a mirror of the amount of gas present in the local volume, but likely reflects other features as well, such as underlying pathological alterations of lung tissue or regional blood flow. The preliminary studies presented here are clearly insufficient to address such issues as the extent to which variations in perfusion might manifest as measureable changes in the dissolved-phase signal intensity, but they nonetheless point to a substantial potential for investigating lung function and disease using this technique.

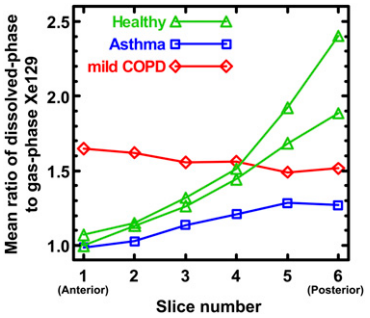

Fig. 4. Variation in the mean ratio of dissolved-phase to gas-phase Xe129 with slice position differed greatly between subjects with lung disease and healthy subjects. Mean ratios were calculated from the central six images of 3D acquisitions of the whole lung in subjects 8 and 11 (healthy), subject 7 (asthma), and subject 10 (mild COPD). In the healthy subjects, the ratio increased substantially along the anterior-posterior direction.

The data on the ratio of dissolved-phase to gas-phase Xe129 provide additional support for the potential of this technique. The effect of gravity on the supine lung has been detected previously in healthy subjects using hyperpolarized He3 diffusion imaging as a decrease in apparent diffusion coefficient from the anterior to posterior portion of the lung. However, the change in the apparent diffusion coefficient was ≈30% (18), whereas the change in the ratio of dissolved-phase to gas-phase Xe129 along the anterior-posterior direction in healthy subjects was roughly 100% (Fig. 4). More important, however, are the intriguing variations in the dissolved-phase to gas-phase ratio shown in Fig. 4 for two subjects with lung disease. These differ markedly from those seen in the healthy subjects, presumably due to structural or functional lung changes resulting from disease. It is important to note, however, that values for the ratio of dissolved-phase to gas-phase Xe129 and the associated anterior-posterior gradient depend on the degree of lung inflation. Specifically, the ratios in the middle and posterior sections of the lung should decrease as lung inflation increases, causing the anterior-posterior gradient to decrease as well. Thus, if the lungs of a subject with disease were somewhat hyperexpanded at baseline, then the resulting gradient would be expected to be lower than that of a healthy subject performing an equivalent breathing maneuver. Regardless, a possible difference in the degree of lung inflation between subject 10 (mild COPD) and the healthy subjects does not explain the elevated ratio values seen in the anterior portion of the lung in subject 10 (Fig. 4). In general, performing future experiments using an MRI-compatible spirometer to permit better control over the degree of lung inflation may be valuable.

The decoupling of ventilation and dissolved-phase signals for certain circumstances is further highlighted by the results in the healthy volunteer who had an incidental finding of a small pulmonary nodule, which appeared as a very bright focus in the dissolved-phase component of the MRI images. Clearly, hyperpolarized Xe129, transported through the vasculature, was concentrated in the region of the nodule over the course of the breath-hold acquisition. The signal contribution from Xe129 in the blood that has traveled to a location distant from the airspaces, such as to a solid lesion or the major vessels and heart, should depend on the frequency and amplitude of radiofrequency excitation (6, 9, 10). Thus, by selecting appropriate acquisition parameters, it should be possible to highlight Xe129 that has just dissolved in tissue versus Xe129 that has been transported away from the airspaces. Furthermore, the chemical shift difference between Xe129 in lung tissue and that in red blood cells is sufficiently large (~20 ppm in humans) to permit selective suppression or excitation of one of these signal sources using established strategies, thereby providing another means to tease out the relative contributions of the different compartments that compose the dissolved-phase signal.

The chemical shift difference between Xe129 in tissue and that in red blood cells is expected to provide another mechanism for exploring the relative contributions of these compartments. It is well known in clinical MRI that a chemical shift difference between two components leads to oscillatory signal decay as a function of echo time for image voxels containing a mixture of the components. The relative contributions of the components can be assessed by collecting gradient-echo images wherein the echo time is chosen to correspond to one of the periodic times when the complex signals are aligned in the same direction ("in-phase") or in opposite directions ("opposed-phase"). For the studies presented here, we chose an echo time approximately equal to the first in-phase time for Xe129 in tissue and red blood cells.

Although 2D projection acquisitions provided images with relatively high signal-to-noise ratios, spatial encoding in the third dimension is highly desirable for investigating lung function and disease, which are inherently spatially heterogeneous. The 3D acquisitions demonstrated that the acquisition of multiple image sections within the lung is feasible; however, these images had relatively low resolution compared with routine clinical images from proton-based MRI. Nonetheless, several avenues exist for substantially improving the Xe129 images using our technique. Ongoing efforts suggest that gas polarizations approximately double those achieved in our studies can be expected in the near future (12). Such a polarization—and hence signal—improvement could be traded for increased spatial resolution. Furthermore, we expect that optimization of the frequency and amplitude of radiofrequency excitation will be important for maximizing dissolved-phase signal levels. Finally, 3D acquisitions are ideally suited for a compressed-sensing approach (19). As recently demonstrated for other MRI applications (19, 20), compressed sensing is well suited for both accelerating the acquisition, which would provide more flexibility in the selection of timing parameters to highlight selected compartments, and improving the signal-to-noise ratio due to the inherent denoising properties of the reconstruction.

As indicated by Eq. [**1**] (*Materials and Methods*), spatial resolution and receiver bandwidth are inherently linked. As a result, decreasing the voxel size (increasing spatial resolution) requires decreasing the bandwidth as well, which in turn increases chemical shift displacement between the red blood cell and tissue components along the frequency-encoding direction, and also increases sensitivity to main field inhomogeneity. Strategies for overcoming this limitation are under evaluation. Another limitation of the current implementation is that the flip angles for the gas-phase and dissolved-phase components are directly coupled; changing the flip-angle value for the gas phase relative to that for the dissolved phase requires redesign of the radiofrequency pulse waveform. An improved approach would be to independently design the excitation characteristics for the gas-phase and dissolved-phase frequency ranges.

Chemical shift imaging (10, 21) is another MRI acquisition method that can provide gas-phase and dissolved-phase images. Chemical shift acquisitions demonstrated in rats using hyperpolarized Xe129 required many breaths of gas over a period of several minutes to yield 2D projection images (10), although chemical shift images have been demonstrated in rabbits using single breath-hold techniques (22). Chemical shift imaging has the advantage of yielding data from which images for each resonance can be estimated; however, for typical image sizes, the method requires at least an order of magnitude increase in the number of radiofrequency excitations, which fundamentally limits flexibility in choosing measurement parameters, especially for 3D acquisitions. However, by combining spatial and spectral encoding using an echo-planar readout (23), chemical shift imaging acquisition can be accelerated significantly. Although implementing the original form of this method for dissolved-phase hyperpolarized Xe129 would be challenging because of the relatively short T2* MRI values, optimized versions using least squares decomposition (24), which substantially reduces the required number of echoes, might have potential for application to hyperpolarized Xe129 lung imaging.

In conclusion, we have demonstrated an imaging method for the human lung that permits both simultaneous observation of the 3D distributions of ventilation and gas uptake and quantification of regional gas uptake in a single short acquisition that can be easily tolerated by subjects with lung disease. This method provides opportunities for quantifying relationships among gas delivery, exchange, and transport and appears to have significant potential to broaden our understanding of lung disease. Our results, although obtained from a small number of subjects, suggest differences in the spatial variations in gas uptake and ventilation in subjects with asthma and COPD. We speculate that this discordance is due to regional alterations in tissue status (COPD) or blood flow (COPD and asthma) that are unrelated to local ventilation, and suggest that improved understanding of alterations in regional gas uptake may provide fresh insights into the relative incongruity in some subjects between subjective symptoms and the results of current primary tests for assessing the severity of lung disease, such as spirometry.

Materials and Methods

Acquisition Parameters to Separate Gas-Phase and Dissolved-Phase Xe129. To achieve the desired separation in the image between the gas and dissolved components along the frequency-encoding direction, the chemical shift difference (Δf_{G-LP}) between Xe129 in the airspaces and Xe129 dissolved in the lung parenchyma must exceed the frequency bandwidth of the lung (Δf_{lung}) (Fig. 1*C*). The chemical shift difference, Δf_{G-LP}, expressed in Hz is $\gamma B_0 \Delta\chi_{G-LP}$, where γ is the gyromagnetic ratio for Xe129 (in MHz/T), B_0 is the static magnetic field strength (in T), and $\Delta\chi_{G-LP}$ is the chemical shift difference (in ppm). On a typical clinical MRI unit, the receiver bandwidth can be directly specified and the spatial resolution (i.e., pixel dimensions) can be specified via the field-of-view and matrix size. In these terms, the frequency bandwidth of the lung can be expressed in Hz as BW $W_L/\Delta x$, where BW is the receiver bandwidth (in Hz/pixel), W_L is the width of the lung (in mm), and Δx is the pixel dimension along the frequency-encoding direction (in mm). Assuming that a desired value for Δx is selected, the requirement for the receiver bandwidth is

$$\mathrm{BW} < \frac{\gamma\, \mathrm{B}_0\, \Delta\chi_{\mathrm{G-LP}}\, \Delta x}{W_L}. \qquad [1]$$

For example, at 1.5 T and a value of 10 mm for Δx, and assuming that the lung is 240 mm wide, the receiver bandwidth must be <146 Hz/pixel, which is within the range of values typically used for clinical MRI.

The double outline of the lung for the dissolved-phase component in Fig. 1*C* illustrates that the signal from the red blood cell compartment should appear slightly shifted relative to that from the lung parenchyma compartment, due to the chemical shift difference between the corresponding resonances. Nonetheless, this shift may not be appreciated in the image if the spatial resolution is relatively low, or if the signal from one compartment is much larger than that from the other compartment.

Human Subjects. All experiments were performed under a physician's Investigational New Drug application for imaging with hyperpolarized Xe129 using a protocol approved by the University of Virginia's Institutional Review Board. The details of the study procedure, including associated risks and benefits, were explained to each subject, and written informed consent was obtained before enrollment in the study. Spirometry was performed immediately before MRI using a hand-held device (Koko; PDS Ferraris). Twelve-lead electrocardiography (HP Pagewriter Xli) was performed immediately before and immediately after MRI. Throughout the MRI session, the subject's heart rate and oxygen saturation level were recorded (3150 MRI Patient Monitor; Invivo Research), and the subject was monitored for central nervous system side effects of the inhaled xenon. All studies were supervised by a physician.

MRI Measurements. MRI was performed on a 1.5-T whole-body commercial scanner (Magnetom Avanto; Siemens) that included the multinuclear imaging option and a flexible chest radiofrequency coil (Clinical MR Solutions) tuned to the Xe129 resonant frequency. Using the scheme outlined in Fig. 1, a simultaneous gas-phase–dissolved-phase imaging technique was implemented based on a standard radiofrequency-spoiled gradient-echo pulse sequence. Considering that the signal evolutions depend on the repetition

time and flip angles, and that the signal amplitudes may decrease markedly during the course of the acquisition as the hyperpolarized magnetization is depleted (13), sequential, rather than centric, phase-encoding order was used, to reduce associated image blurring. The desired response for the excitation radiofrequency pulse (Fig. 1*B*) was obtained by systematically adjusting the timing parameters for a truncated-sinc waveform and then evaluating the resulting response as predicted by the Bloch equations. The MRI acquisition parameters are listed in Table S1. Acquisition (breath-hold) times were between 2 and 18 s.

Enriched xenon gas (87% Xe129) was polarized by collisional spin exchange with an optically pumped rubidium vapor using a prototype commercial system (Xemed) that provided gas polarization of ≈30%. Immediately before imaging, 0.1–1 L of hyperpolarized Xe129 gas was dispensed into a Tedlar bag (Jensen Inert Products) and connected to one arm of a plastic Y connector. A second Tedlar bag containing a mixture of room air and medical-grade oxygen was connected to the other arm of the Y connector. The volumes and relative fractions of room air and oxygen were selected so that the gas mixture inhaled through the base of the Y connector contained 21% oxygen.

Each subject was positioned supine on the scanner table with the Xe129 radiofrequency coil around the chest; imaging typically began within 10 min of positioning. Using conventional proton MRI and a breath-hold acquisition, "scout" images were obtained for positioning of the Xe129 acquisitions. Next, the subject inhaled a gas mixture containing ≈0.1 L of hyperpolarized Xe129 from maximum expiration, and a breath-hold acquisition was performed for scanner calibration. Finally, for each of the breath-hold imaging acquisitions, the subject inhaled a gas mixture containing either 0.5 L of hyperpolarized Xe129 and 0.24 L of an air–oxygen mixture (subjects 1–10) or 1 L of hyperpolarized Xe129 and 0.47 L of an air–oxygen mixture (subject 11), from maximum expiration.

Ratio of Dissolved-Phase to Gas-Phase Xe129. In four subjects in whom 3D acquisitions were performed using identical parameters (subjects 7, 8, 10, and 11), the ratio of the signal intensities for dissolved-phase Xe129 to those for gas-phase Xe129 was calculated. The approximate shift along the frequency-encoding direction for the dissolved-phase component relative to the gas-phase component is indicated by the associated chemical shift difference. The exact shift used for ratio calculations was determined for each subject by performing a cross-correlation between the dissolved-phase and gas-phase components of a representative image. Background noise was masked from the images using an intensity threshold. The ratio was calculated on a pixel-by-pixel basis for each slice in each image set, and the mean ratio value was determined for each slice.

ACKNOWLEDGMENTS. This work was supported by National Institutes of Health Grants R41 HL091578, R01 EB003202, and R01 HL079077 and by a research grant from Siemens Medical Solutions.

1. Möller HE, et al. (2002) MRI of the lungs using hyperpolarized noble gases. *Magn Reson Med* 47:1029–1051.
2. Abraham MH, Kamlet MJ, Taft RW, Doherty RM, Weathersby PK (1985) Solubility properties in polymers and biological media, 2: The correlation and prediction of the solubilities of nonelectrolytes in biological tissues and fluids. *J Med Chem* 28:865–870.
3. Miller KW, et al. (1981) Xenon NMR: chemical shifts of a general anesthetic in common solvents, proteins, and membranes. *Proc Natl Acad Sci USA* 78:4946–4949.
4. Ruppert K, Brookeman JR, Hagspiel KD, Mugler JP, 3rd (2000) Probing lung physiology with xenon polarization transfer contrast (XTC). *Magn Reson Med* 44: 349–357.
5. Driehuys B, et al. (2006) Imaging alveolar-capillary gas transfer using hyperpolarized 129Xe MRI. *Proc Natl Acad Sci USA* 103:18278–18283.
6. Sakai K, et al. (1996) Temporal dynamics of hyperpolarized 129Xe resonances in living rats. *J Magn Reson B* 111:300–304.
7. Wagshul ME, et al. (1996) In vivo MR imaging and spectroscopy using hyperpolarized 129Xe. *Magn Reson Med* 36:183–191.
8. Mugler JP, 3rd, et al. (1997) MR imaging and spectroscopy using hyperpolarized ^{129}Xe gas: Preliminary human results. *Magn Reson Med* 37:809–815.
9. Ruppert K, Brookeman JR, Hagspiel KD, Driehuys B, Mugler JP, 3rd (2000) NMR of hyperpolarized (129)Xe in the canine chest: Spectral dynamics during a breath-hold. *NMR Biomed* 13:220–228.
10. Swanson SD, Rosen MS, Coulter KP, Welsh RC, Chupp TE (1999) Distribution and dynamics of laser-polarized $^{(129)}$Xe magnetization in vivo. *Magn Reson Med* 42: 1137–1145.
11. Wakayama T, Narazaki M, Kimura A, Fujiwara H (2008) Hyperpolarized 129Xe phase-selective imaging of mouse lung at 9.4T using a continuous-flow hyperpolarizing system. *Magn Reson Med Sci* 7:65–72.
12. Hersman FW, et al. (2008) Large production system for hyperpolarized 129Xe for human lung imaging studies. *Acad Radiol* 15:683–692.
13. Cleveland ZI, et al. (2010) Hyperpolarized Xe MR imaging of alveolar gas uptake in humans. *PLoS ONE* 5:e12192.
14. MacFall JR, et al. (1996) Human lung air spaces: Potential for MR imaging with hyperpolarized He-3. *Radiology* 200:553–558.
15. Kauczor HU, et al. (1996) Normal and abnormal pulmonary ventilation: Visualization at hyperpolarized He-3 MR imaging. *Radiology* 201:564–568.
16. de Lange EE, et al. (1999) Lung air spaces: MR imaging evaluation with hyperpolarized ^{3}He gas. *Radiology* 210:851–857.
17. Altes TA, et al. (2001) Hyperpolarized ^{3}He MR lung ventilation imaging in asthmatics: Preliminary findings. *J Magn Reson Imaging* 13:378–384.
18. Fichele S, et al. (2004) MRI of helium-3 gas in healthy lungs: Posture-related variations of alveolar size. *J Magn Reson Imaging* 20:331–335.
19. Lustig M, Donoho D, Pauly JM (2007) Sparse MRI: The application of compressed sensing for rapid MR imaging. *Magn Reson Med* 58:1182–1195.
20. Hu S, et al. (2008) Compressed sensing for resolution enhancement of hyperpolarized ^{13}C flyback 3D-MRSI. *J Magn Reson* 192:258–264.
21. Brown TR, Kincaid BM, Ugurbil K (1982) NMR chemical shift imaging in three dimensions. *Proc Natl Acad Sci USA* 79:3523–3526.
22. Mata J, et al. (2010) Quantification and temporal study of physiologic lung changes in animal models of lung disease using 2D and 3D-CSI with Xe-129 (abstract). *Proc Int Soc Magn Reson Med* 18:989.
23. Posse S, Tedeschi G, Risinger R, Ogg R, Le Bihan D (1995) High-speed ^{1}H spectroscopic imaging in human brain by echo planar spatial-spectral encoding. *Magn Reson Med* 33:34–40.
24. Reeder SB, Brittain JH, Grist TM, Yen YF (2007) Least-squares chemical shift separation for $^{(13)}$C metabolic imaging. *J Magn Reson Imaging* 26:1145–1152.